Advanced Microstructure Characterization and Analysis of Naturally Occurring Boron-Rich Silicate Material: Tourmaline

Sneha Dandekar[1*], Dilip Peshwe[1]
[1]Department of Metallurgical and Materials Engineering, VisvesvarayaNational Institute of Technology, Nagpur, Maharashtra, India

Abstract:
The boron-rich silicate material (BMS)/tourmaline isa technologically important material in pressure devices. In the present work, the BSM was extracted from the tailings of an alumino-silicate treating plant using extractive metallurgy processes. The material was studied in detail using different characterization techniques like X-ray diffraction (XRD), Raman Spectroscopy, Scanning Electron Microscopy (SEM), Energy Dispersive Spectroscopy (EDS), Electron Probe Microanalysis (EPMA), and Electron Backscattered Diffraction (EBSD) along with petrographic studies. EBSD analyses give information about crystallographic orientation in the microstructure and dislocation structures produced by deformation. However, it also deals with the various application of tourmaline, depending on the particle size of the material in the electrical, chemical as well as medical industries.
Keywords: Tourmaline, alumina-silicate, tailings, extractive metallurgy, microstructures.

1. Introduction:

As the most ample mine waste material, the tailings from mines in India have been calculated to have a total mass of more than 170 million tons, which inhabits a lot of valuable agricultural land. The use of tailings as novel wealth has become one of the trending topics and is a real challenge faced by the mining industry.

Tourmaline is a complex borosilicate mineral with (K, Na, Ca, vacancy) (Al, Li, Fe^{+2}, Mn^{+2}, Mg, Fe^{+3}, V^{+3}, Cr^{+3},)$_3$ (Al, Mg, Fe^{+3}, Cr^{+3}, V^{+3})$_6$ (Si, Al, B)$_6$ O_{18} (BO_3)$_3$ (OH, O)$_3$ (OH, F, O) as an empirical formula (Hawthorne and Henry, 1999). It crystallizes in an orthorhombic crystal system and occurs in prismatic or columnar form [1]. It is used in pressure devices because of its piezoelectric properties; its ability to change in shape when voltage is applied or it generates electric charge under mechanical stress. The extraction of BMS from the tailings was done by using physical extraction methods such as ball-milling and gravity separation methods. The application of tourmaline varies, depending on the particle size of the material.

This paper deals with the extraction of tourmaline from mine tailing, in order to achieve zero-waste mining, and a few non-destructive testing methods such as its characterization, and microstructural analysis. This study has been completed with the extraction technique of BSM from its ore and microstructural characterization depending on its surface morphology, crystal size, crystal structure, elemental composition phase identification and quantification and misorientation of the grains.

2. Materials and Analysis:

A flow chart of the experimental methods implemented to carry out the current study is shown in Figure 1. The tailing samples were collected from the alumina-silicate mine (latitude 79.93° N; and longitude 21.05° E) of Sakoli tehsil, Bhandara district of Maharashtra. The samples were then processed to extract tourmaline by means of ball-milling and gravity separation techniques.

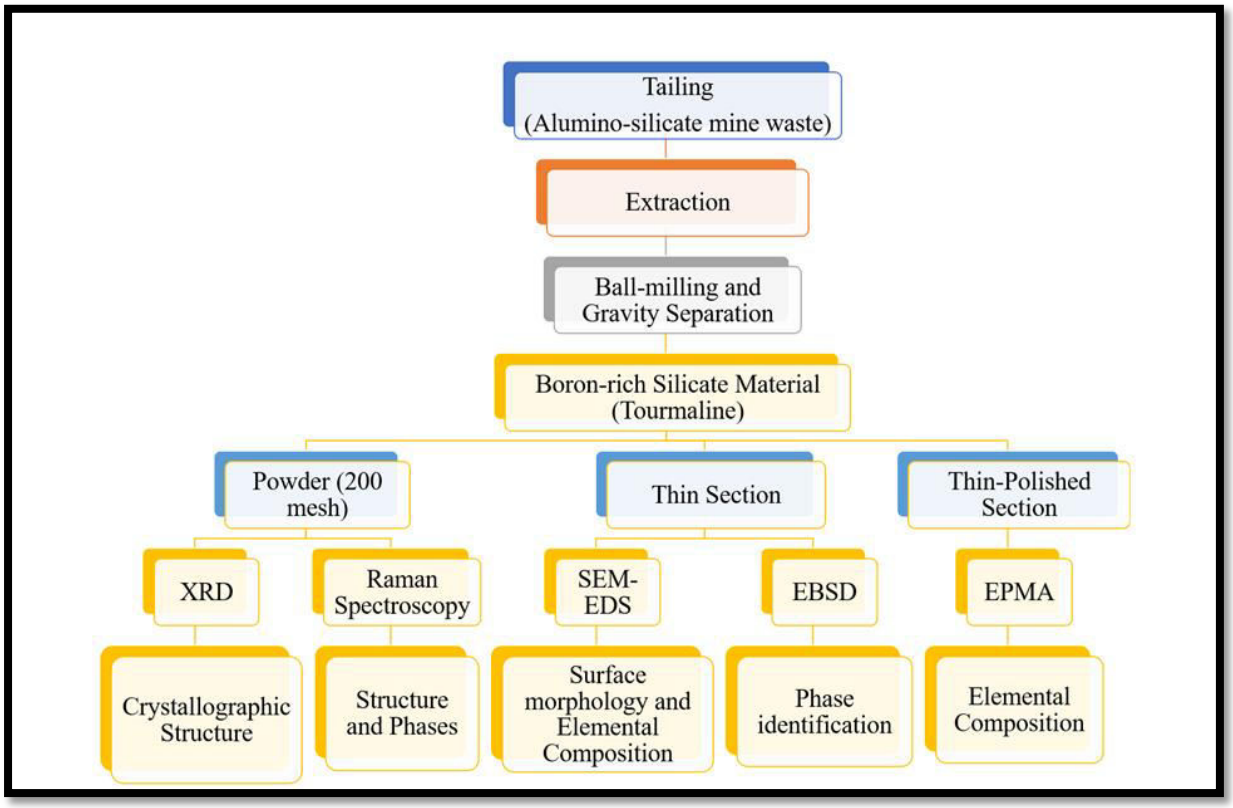

Figure 1: Flow chart showing analysis methods used for characterization of the BSM

Properly BMS were prepared and thin polished sections of the samples were prepared to study the electron probe microanalysis (EPMA) of the material. The study was performed using a CAMECA SX-100 analyser at the National Centre of Excellence in Geoscience Research (NCEGR), GSI, Bangalore. The spectra were met using column condition of abeam current of 15 nA, acceleration voltage of 15 keV and beam size of 1 μm. CAMECA SX- 100 Peak Sight-Geo Quanta software package was used for standardization, quantification and overlap correction.

Some chunks of the sample were powdered using a ball milland extracted by gravity separation equipment such as a jaw crusher, and, shaking table, which were again sieved to 200 mesh sizefor XRD and Raman spectroscopy study. XRD patterns were obtained by means of a PanalyticalX'Pert Pro MPD diffractometer with CuKα radiation (λ = 1.54 Å) made at a current of 40 mA voltage of 40 kV. Scanning was completed in the angular range of 5–80°, 2θ with a time per step of 15 s and scan step size 0.01°. Raman Spectroscopy was done by means of a Raman spectrometer (NOST: HEDA-URSM-4/5/7). 523 nm laser was used to stimulate the sample at room temperature. Two different laser intensities were used to study the difference in vibration of molecules at different intensities.

For SEM-EDS and EBSD, the samples were cut into small sections of 10x 10x3 mm size. It was then polished as per standard polishing technique using fine silicon carbide abrasive paper up to 2500 grit. It was then polished on velvet cloth using an alumina slurry of 1 μm, followed by a polycrystalline diamond suspension of 0.25 μm to obtain a mirror finish. The structural changes were studied using a scanning electron microscope (SEM-JEOL 6830A). Using auto sputter (JOEL-JFC 1600 auto fine coater), the material was treated with a thin gold-palladium coatingfor the study of exterior morphology. The EBSD maps were acquired with an OXFORD EBSD system attached on a JEOL 7600F FEG (Field Emission Gun) SEM, operated at 20 kV and probe current 18 A in focused beam mode.

3. Results and Discussion

3.1. X-Ray diffraction:

From the analysis of the diffractogram (figure 2), it was found that the peak at 2θ angles of 24.01°, 33.09°, 39.50°, 40.31°, 40.72°, 50.16°, 59.96°, 67.22°, 68.17°, 81.32°, 90.84° were for BSM. The obtained analysed data of the XRD diffractogram ascertains the fact that the crystals of BSM are orthorhombic which indeed is confirmed by the JCPDS data (01-074-1731). The hkl planes confirmed the crystal class is dipyramidal (orthorhombic) (mmm) (Vrána, 1979).

The crystallite size was calculated by means of the Debye-Scherrer formula [2]:

$$D = \frac{0.9\lambda}{B\cos\theta}$$

where D represents the arithmetic average of the size of the crystalline domain, for the wavelength of CuK_{α}, λ is 1.54 Å, B represents full-width half maximum (FWHM) and θ is the Bragg's angle. Calculating the crystallite size by means of the above formula, it was found to be ~2.9378 nmin size.

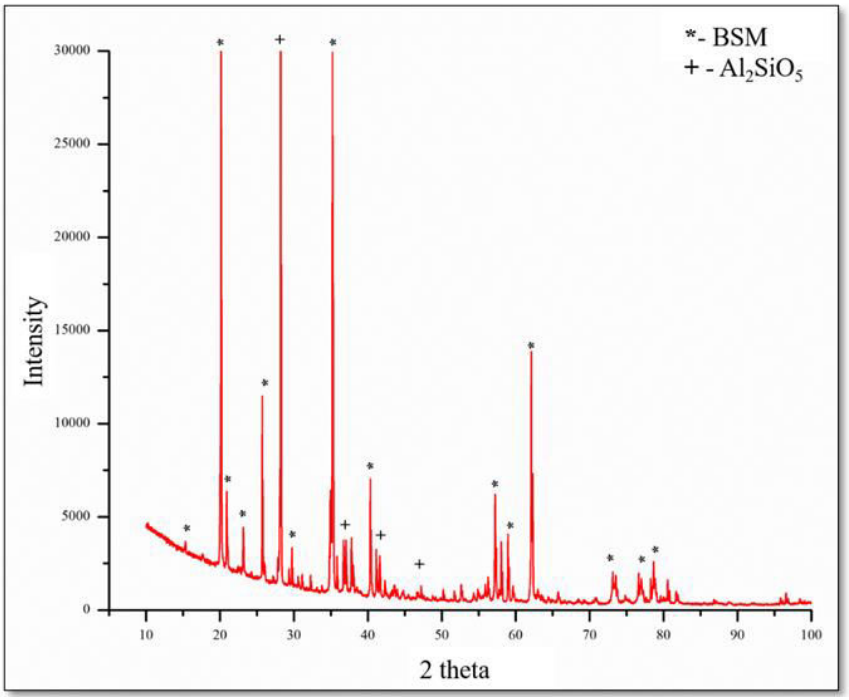

Figure 2: X-Ray diffractrogram of the sample

3.2Raman spectroscopy:

The Raman spectra of the sample were recorded at the wavelength of 532 nm in the background region of 0 to 2000 cm^{-1}. In order to measure the detail peaks spectra were generated with 20% and 30% of laser intensity for 20 and 15 seconds for each intensity, however, the average spectra are reported (figure 3). The Raman shifts to the elongating vibration of the B–O bonds in the BO_3 triangles can be allocated above 1200 cm^{-1}. The peaks between 800 and 1100 cm^{-1}comprise Si–O, B–O, Al–O stretching, BO_3 bending, O–Al–O motion, as well as AlO_6 and BO_3 deformations modes. The strong band of symmetrical Si–O–Si vibration is found at ~600–800 cm^{-1}. As per the calculation of Reddy (2007), the Si_6O_{18} ring can be measured a separate unit, with its internal shaking modes being subtle to the neighbouring cations of the ring. The Al–O and Y–O bond stretching modes are centred at 400–600 cm^{-1}. Whereas, the X–O bond stretching is observed at wavenumbers less than 400 cm^{-1}[3, 4]. The presence of two bands at ~560 and ~611 cm^{-1} in the Raman spectrum of the BSM may also specify the presence of [5] BO_3 in the BSM structure [6]. The Raman spectra of the BSM crystals exhibit peaks at 630–690 cm^{-1}, which are indicative features of tourmaline [7].

The shift of BO_3 was found to be on a lower wave number (blue-shift), which is due to the formation of a short bond length in the crystal. Fe^{2+} cation indicates an exceptional peak at 355cm $^{-1}$. As the Fe is occupied in Y_3-site of tourmaline structure [8],and BO_3 is attached with the Y_3-site [9].

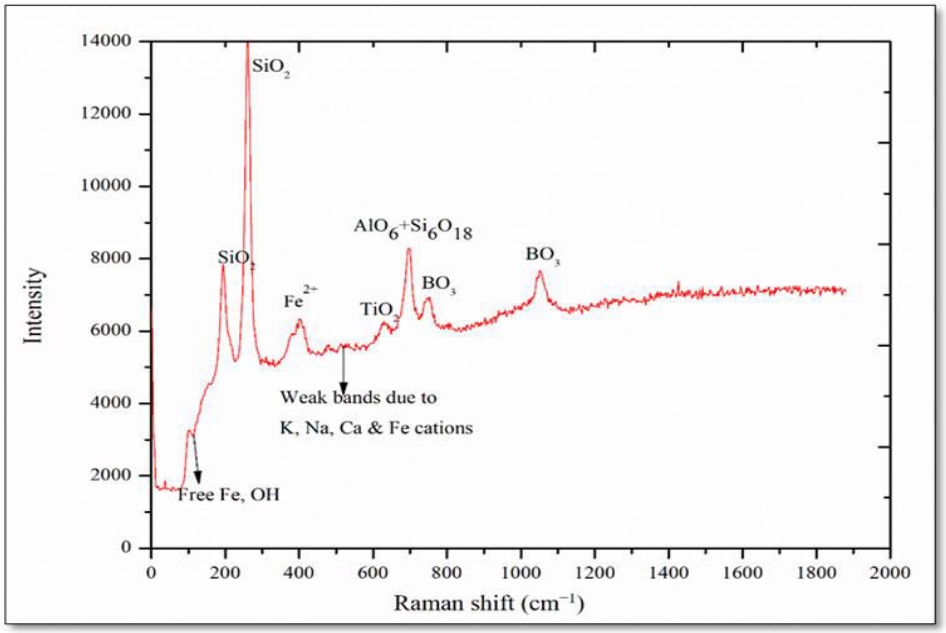

Figure 3: Raman Spectra of the BSM sample

3.3 Scanning electron microscopy:

Figure 5 shows the superficial morphology of the sample. The formation of orthorhombic-shaped BSM crystals has been perceived in SEM (figure 4a). Though, at some places, tourmaline is found in well-crystallized hexagonal-shaped along with Al_2SiO_5 (figure 4b). Whereas, the EDS data (figure 4 c and d) represents the elemental composition of the sample which assures the extraction of BSM from the tailings.

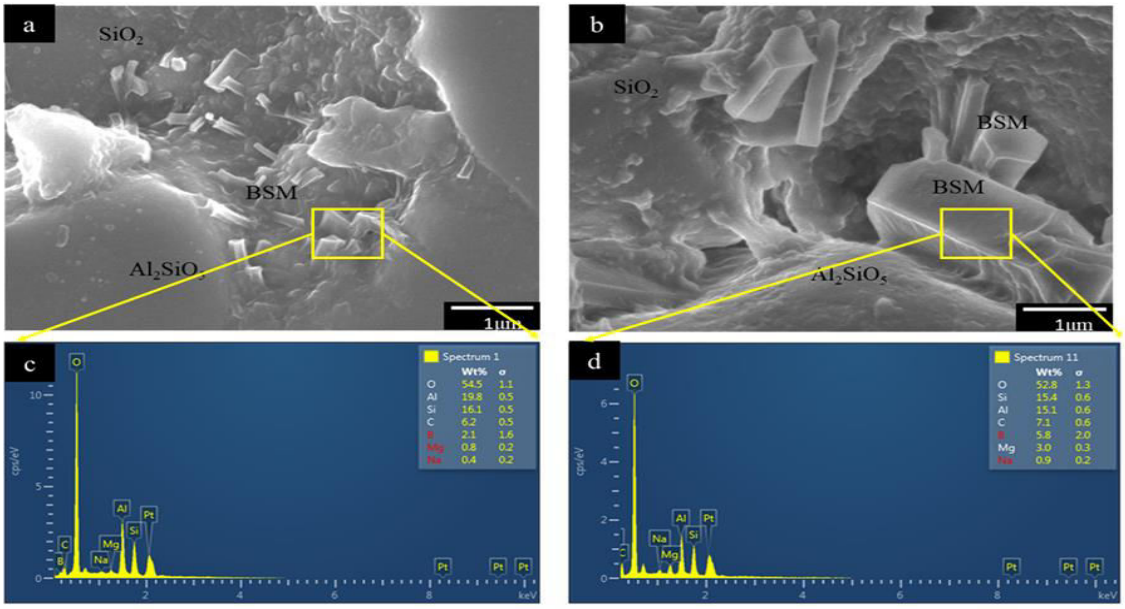

Figure 4: SEM images of the sample

3.4 EPM analysis of BSM:

The EPMA study revealed that the BSM sample is almost of homogeneous composition (Table 1). The mineral has highest content of Al_2O_3 (58.71 -59.59 wt %), SiO_2 (29.65 -34.44 wt %), TiO_2 (1.75 -1.95 wt %) and FeO and MgO in less amount (0.3 -0.5 wt %). It was found that, Al_2O_3, and TiO_2 are comparatively higher than that of standard BSM[10, 11].However, at some point BSM shows composition change within the crystal. The Al_2O_3 (35.49 -36.97 wt %), SiO_2 (34.5 -35 wt %), FeO (8.52-9.01 wt %), MgO (3.06-3.61 wt %) and Na_2O (1.35-1.44 wt %) whereas, CaO, K_2O is are almost constant and do not exceed 0.5 wt%, here it shows the more amount of FeO content.

3.5 Electron backscattered diffraction:

Due to the micro size of the minerals and their intergrowth with other minerals, single-crystal X-ray diffraction studies could not be carried out. Hence, the three minerals were characterized by electron backscattered diffraction (EBSD). Electron backscatter diffraction patterns at a sub-micrometre scale were taken by an OXFORD camera attached to the scanning electron microscope, which was operated at 20 kV with a probe current 18 A in focused beam mode [12, 13].

The cell constants were obtained from the literature and the mineral arrangement was determined by conforming the experimental EBSD pattern to the standard BSM[16-18]. In the instance of each of the new minerals, EBSD patterns (Figure 5) were indexed with the BSM structure to give the finest fit based on unit-cell data for BSM from [16]. These matches confirmed that BSM has similar unit-cell parameters to, Pnma (no. 62)space group, and unit-cell parameters near to those obtained by Moore and Araki (1978) for BSM: a = 4.6948 A˚, b = 11.8037 A˚, c = 20.2106 A˚, with V = 1119.99 A˚ 3 and Z = 4. The inverse-pole figure, Kernel average misorientation, and Phase map were studied using the technique.

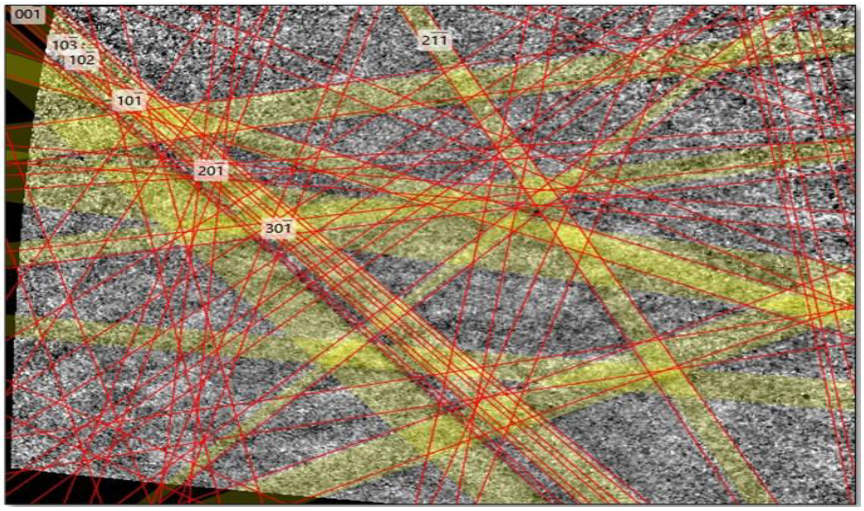

Figure 5: EBSD pattern of the BSM

3.5.1 The inverse-pole figure (IPF):

The IPF shows the different grains of different colour in the sample that has similar orientation as shown in similar colours. The IPF is studied in Y-scheme which shows the colouring of each point according to which crystal direction is parallel to Y direction of the map. In figure 6 (a) large area is covered in blue, which interprets as the c-axis of the coarse crystal is predominantly lining up with the Y-axis of the map. The Al-rich BSM grains (figure 6b) are almost blue in colour, representing the grains are oriented in the (010) plane, whereas, green coloured grains show (100) orientation and red shows (001) orientation of the grains. Fe-rich BSM/ tourmaline grains are arranged in (0001) plane, parallel to the y direction of the map. The blue colour grains are perpendicular to the Y direction (figure 6c). However, the Al_2SiO_5grains (figure 6 d) are arranged in (010) plane and SiO_2crystal are oriented in (0001) plane (figure 6e).

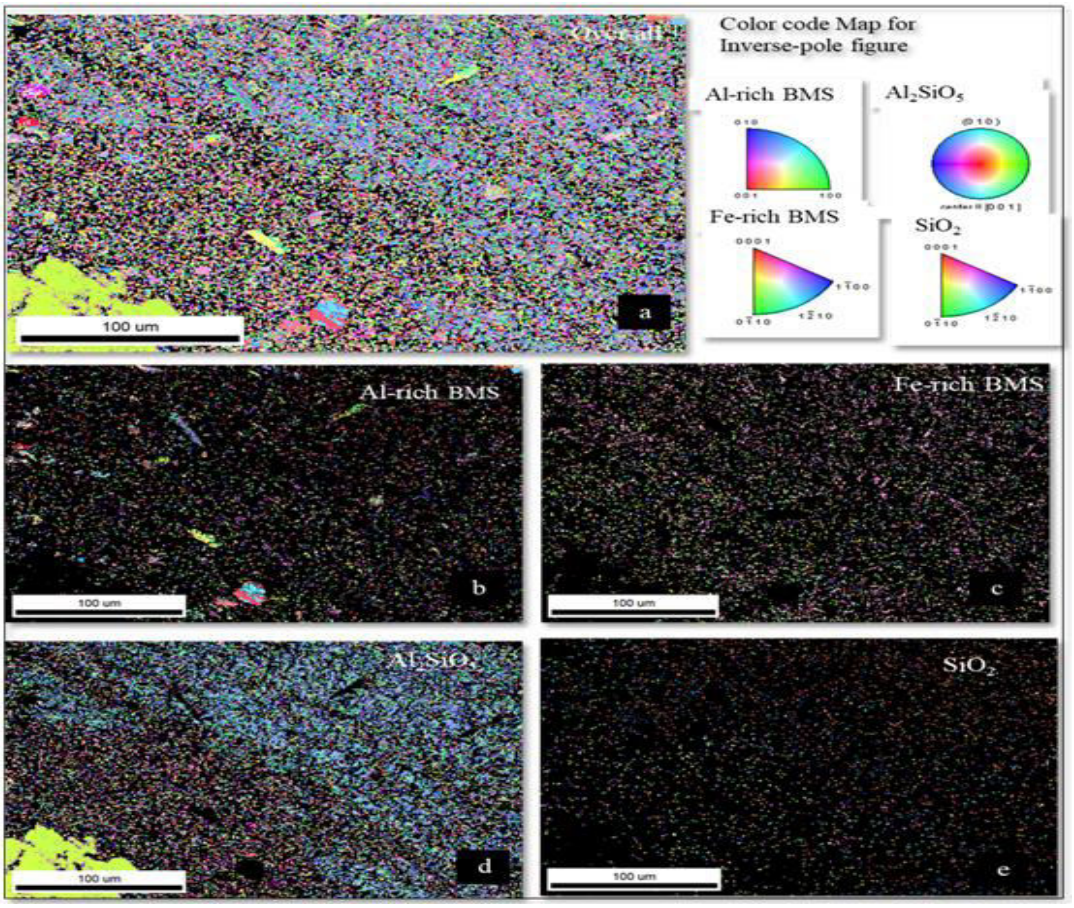

Figure 6: Inverse-pole figure (IPF) of the sample

3.5.2 Phase identification:

EBSD is a good tool for phase identification and to study the dissemination of different phases of minerals. Phases can be represented on a map, highlighting their distribution and providing accurate area fractions for each phase. From figure 7, it can be analysed that the majority of the grains are of Al_2SiO_5 0.412 total fraction followed by Al-rich BSM that is 0.117, Fe-rich BSM/ tourmaline 0.112, and SiO_2 0.046 fraction.

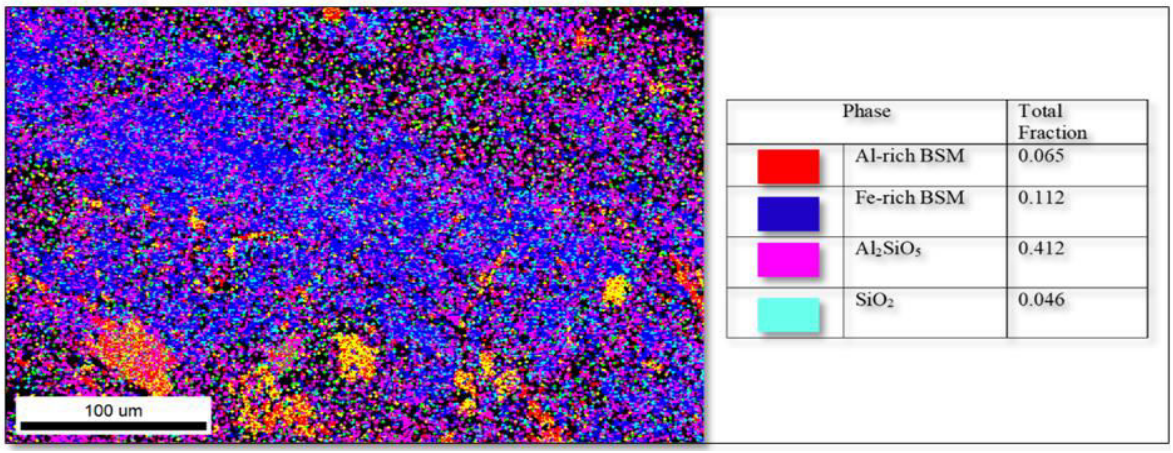

Figure 7: Phase Map (PM) of the BSM

3.5.3 Kernel average misorientation (KAM):

KAM can be employed as an amount of local grain misorientation. KAM calculates the average misorientation around a dimension site in relation to a predefined collection of nearest neighbour points. The local misorientation ascribed to the core point of a certain grain with respect to all locations on the

kernel's edge is measured in this mode. Because of the greater dislocation density, KAM is often high in distorted grains [17]. KAM analysis may indicate stockpiled strain energy in the grain because it helps to comprehend local lattice distortions, high dislocation density and confined deformation. In Figure8, most of the area is covered with blue colour which represents lower or negligible local misorientation with neighbours. However, few areas are identified as green zone and correspond to comparatively higher local misorientation with neighbour. Whereas, the red colour zone represents the highest local misorientation with the neighbour.

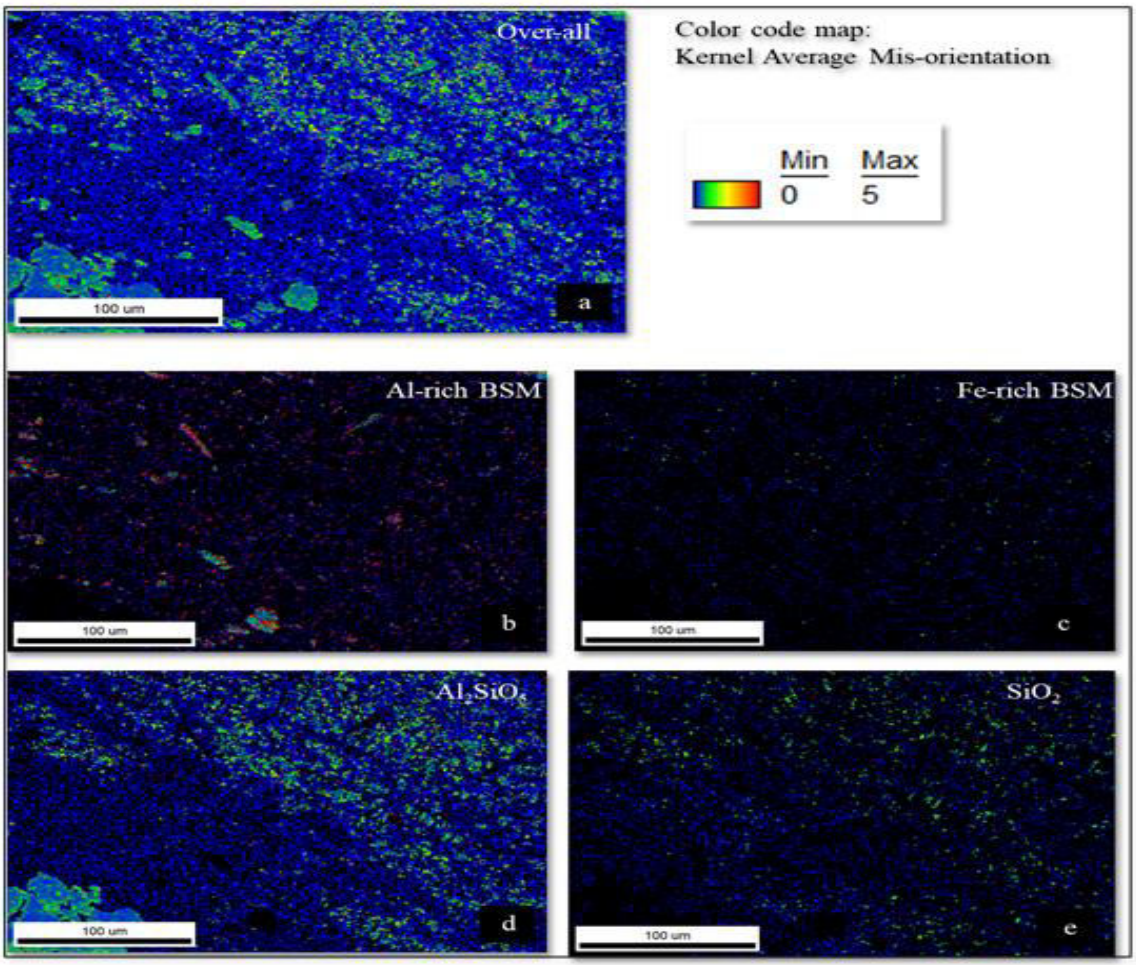

Figure 8: Kernal Average Mis-orientation (KAM) of the sample

4. Concluding Remarks:

Through the extraction of boron-rich silicate materials from the tailings of the alumina-silicate processing plant, it is found that,

4.1. There are two types of BSM present in the tailings which are Al-rich and Fe-rich in nature which was confirmed by the EPMA and EBSD study.

4.2. From the total fraction of phases it was found that the Fe-rich BSM/ tourmaline is more, compared to the Al-rich BSM phase.

4.3. The crystals are approximately~2.9378 nm in size and are orthorhombic in shape, whereas the Raman spectra have confirmed the presence of BO_3 in the material.

4.4. This availability of BSM from the study area can be an additional resource for glass, and ceramics industries as the boron acts as a toughening material in these industries and also for pressure devices manufacturing industries.

Conflict of Interest: The authors have no conflicts of interest to declare

5. References:

1. E. S. Grew, 'Borosilicates (exclusive of tourmaline and boron in rock-forming minerals in metamorphic environments. Grew, E.S. and Anovitz, L.M. 9eds.) Boron: Mineralogy and Geochemistry', Rev. in Minerak, 33 (1996), 387-507.
2. Cullity B. D. and Stock S. R. (2001), Elements of x-ray diffraction, 3rd ed , Prentice Hall, Upper Saddle River, NJ, ©2001
3. Hoang L.H., Hien N. T. M., Chen X. B., Minha N. V., and Yang In-S (2010) Raman spectroscopic study of various types of tourmalines, J. Raman Spectrosc., 42, 1442–1446
4. Willner, A.P., Schreyer, W. (1991) A dumortierite-topaz-white mica fels from the peraluminous metamorphic suite of Bushmanland (South Africa). N. Jb. Min. Mh. 1991:223–240
5. Pieczka, A., Evans, R.J., Grew, E.S., Groat, L.A., Ma, C. and Rossman, G.R. (2013) Thedumortieritesupergroup. I. A new nomenclature for the dumortierite and holtite groups. Mineralogical Magazine, 77, 2825-2839.
6. Wunder B, Kutzschbach M, Hosse L, Wilke F D H, Schertl H P, Chopin C (2018) Synthetic [4]B-bearing dumortierite and natural [4]B-free magnesiodumortierite from the Dora-Maira Massif: differences in boron coordination in response to ultrahigh pressure, European Journal of Mineralogy, 30, 471-483
7. Watenphul A, Burgdorf M, Schlüter J, Horn I, Malcherek T, Mihailova B (2016) Exploring the potential of Raman spectroscopy for crystallochemical analyses of complex hydrous silicates: II. Tourmalines, American Mineralogist, 101, 970-985B. D. Cullity and S. R. Stock, Elements of X-ray Diffraction, 3rd edn
8. Bast, R., Scherer, E.E., Mezger, K., Austrheim, H., Ludwig, T., Marschall, H.R., Putnis, A., and Löwen, K. (2014) Boron isotopes in tourmaline as a tracer of metasomatic processes in the Bamble sector of Southern Norway. Contributions to Mineralogy and Petrology, 168, 1069.
9. Berryman, E.J., Wunder, B., Ertl, A., Koch-Müller, M., Rhede, D., Scheidl, K., Giester, G., and Heinrich, W. (2015b) Investigation of synthetic K-dravite, dravite, oxy-uvite, and magnesiofoitite using SREF and Raman spectroscopy. Physics and Chemistry of Minerals, in press,
10. Willner, A.P., Schreyer, W. (1991) A dumortierite-topaz-white mica fels from the peraluminous metamorphic suite of Bushmanland (South Africa). N. Jb. Min. Mh. 1991:223–240
11. Taner M. F. and Martin R. F., (1993) , 'Significance Dumortierite in an Aluminosilicate-Rich Alteration Zone Louvicourt Quebec', Canadian Mineralogist, 31, 137-46.
12. Ma, C. and Rossman, G.R. (2008) Barioperovskite, BaTiO3, a new mineral from the Benitoite Mine, California. American Mineralogist, 93, 154–157. ——— (2009) Tistarite, Ti2O3, a new refractory mineral from the Allende meteorite. American Mineralogist,94, 841–844.
13. Ma, C., Beckett, J.R., and Rossman, G.R. (2009) Allendeite and hexamolybdenum: Two new ultra-refractory minerals in Allende and two missing links. 40th Lunar and Planetary Science Conference, The Woodlands, Texas, Abstract 1402.
14. Moore, P.B. and Araki, T. (1978) Dumortierite,Si3B[Al6.75X0.25O17.25(OH)0.75]: a detailed structure analysis. NeuesJahrbuchfu¨ r MineralogieAbhandlungen, 132, 231- 241.
15. Alexander, V.D., Griffen, D.T. and Martin, J.T. (1986) Crystal chemistry of some Fe- and Ti-poor dumortierites. American Mineralogist, 71, 786-794.
16. Hoskins, B.F., Mumme, W.G. and Pryce, M.W. (1989)Holtite, (Si 2.25 Sb 0.75)B[(Al 6 (Al 0.43 Ta 0.27 X 0.30)O15 m(O,OH) 2.25]: crystal structure and crystal chemistry. Mineralogical Magazine,53, 457-463.
17. H. Xie, D. Lin, Y. Chai, J. Hu, EBSD investigation on the evolution of microstructure and grain boundaries in coarse-grained Ni–48Al upon large deformation at elevated temperature, Intermetallics, 58 (2015), pp. 98-102

Table 1 shows the elemental composition of BSM sample

Sample No	1	2	3	4	5	6	7	8	9	10	11	12
SiO2	30.01	30.34	34.73	30.26	34.5	30.22	29.73	29.65	34.44	30.63	34.97	34.6
TiO2	1.75	1.82	0.24	1.79	0.25	1.92	1.83	1.95	0.33	1.86	0.31	0.3
Al2O3	59.59	59.23	36	59.48	36.97	59.2	58.47	58.71	35.59	59.38	35.49	35.82
FeO	0.51	0.42	9.01	0.54	8.91	0.38	0.34	0.37	8.56	0.47	8.52	8.6
MgO	0.33	0.32	3.06	0.33	3.27	0.38	0.39	0.3	3.27	0.34	3.79	3.61
CaO	0.05	0	0.34	0.02	0.43	0	0.01	0.01	0.35	0.01	0.43	0.48
Na2O	0.02	0.02	1.37	0	1.43	0.03	0	0.01	1.38	0.01	1.35	1.44
K2O	0	0.01	0	0	0.04	0	0	0	0.04	0	0.03	0.03
F	0	0	0.51	0.16	0.71	0	0	0	0.39	0	0.31	0.63
O=F	0	0	0.215	0.067	0.299	0	0	0	0.164	0	0.131	0.265
Total	108.584	108.435	98.578	108.87	99.866	108.452	106.784	107.31	97.797	109.099	98.742	98.933
Si	4.348	4.389	5.731	4.356	5.618	4.367	4.363	4.334	5.73	4.401	5.761	5.691
Ti	0.191	0.198	0.03	0.194	0.031	0.209	0.202	0.214	0.041	0.201	0.038	0.037
Al	10.176	10.097	7.002	10.091	7.095	10.082	10.114	10.115	6.979	10.054	6.89	6.944
Fe2+	0.062	0.051	1.243	0.065	1.213	0.046	0.042	0.045	1.191	0.056	1.174	1.183
Mg	0.071	0.069	0.753	0.071	0.794	0.082	0.085	0.065	0.811	0.073	0.931	0.885
Ca	0.008	0	0.06	0.003	0.075	0	0.002	0.002	0.062	0.002	0.076	0.085
Na	0.006	0.006	0.438	0	0.451	0.008	0	0.003	0.445	0.003	0.431	0.459
Li	0.142	0.195	0.237	0.209	0.243	0.208	0.194	0.199	0.23	0.211	0.201	0.238
F	0	0	0.266	0.073	0.366	0	0	0	0.205	0	0.162	0.328
B	3	3	3	3	3	3	3	3	3	3	3	3
Si(T)	4.348	4.389	5.731	4.356	5.618	4.367	4.363	4.334	5.73	4.401	5.761	5.691
Al(T)	1.652	1.611	0.269	1.644	0.382	1.633	1.637	1.666	0.27	1.599	0.239	0.309
Total(T)	6	6	6	6	6	6	6	6	6	6	6	6
Al(Z)	6	6	6	6	6	6	6	6	6	6	6	6
Total(Z)	6	6	6	6	6	6	6	6	6	6	6	6

Al(Y)	2.525	2.486	0.733	2.447	0.713	2.449	2.477	2.449	0.709	2.455	0.651	0.636
Ti(Y)	0.191	0.198	0.03	0.194	0.031	0.209	0.202	0.214	0.041	0.201	0.038	0.037
V(Y)	0.007	0.001	0	0	0	0.003	0	0.023	0	0	0	0.017
Cr(Y)	0.002	0	0.004	0.002	0.006	0.002	0	0.003	0.018	0.003	0.005	0.003
Mg(Y)	0.071	0.069	0.753	0.071	0.794	0.082	0.085	0.065	0.811	0.073	0.931	0.885
Fe2+(Y)	0.062	0.051	1.243	0.065	1.213	0.046	0.042	0.045	1.191	0.056	1.174	1.183
Total(Y)	2.858	3	3	3	3	2.792	2.806	2.801	2.77	2.789	2.799	2.762
Ca(X)	0.008	0	0.06	0.003	0.075	0	0.002	0.002	0.062	0.002	0.076	0.085
Na(X)	0.006	0.006	0.438	0	0.451	0.008	0	0.003	0.445	0.003	0.431	0.459
Total(X)	0.013	0.007	0.498	0.003	0.535	0.008	0.002	0.004	0.516	0.004	0.513	0.55
X-vac.	0.987	0.993	0.502	0.997	0.465	0.992	0.998	0.996	0.484	0.996	0.487	0.45
H2O(c)	4.005	3.942	2.699	3.858	2.668	3.929	3.879	3.891	2.757	3.945	2.849	2.697
B2O3(c)	11.995	11.988	10.449	12.02	10.569	11.986	11.808	11.852	10.374	12.059	10.482	10.475
Li2O(c)	0.244	0.335	0.354	0.36	0.368	0.357	0.327	0.337	0.341	0.365	0.302	0.356
[OH	3.871	3.812	2.995	3.721	2.926	3.8	3.808	3.806	3.081	3.793	3.151	2.985
F	0	0	0.266	0.073	0.366	0	0	0	0.205	0	0.162	0.328
Total]	3.871	3.812	3.261	3.794	3.292	3.8	3.808	3.806	3.286	3.793	3.312	3.313
OH*	3.5	3.5	3.367	3.464	3.317	3.5	3.5	3.5	3.397	3.5	3.419	3.336
O*	27.129	27.188	27.739	27.206	27.708	27.2	27.192	27.194	27.714	27.207	27.688	27.687
Type	Al-rich	Al-rich	Fe-rich	Al-rich	Fe-rich	Al-rich	Al-rich	Al-rich	Fe-rich	Al-rich	Fe-rich	Fe-rich
Name	Boron-rich silicate material											